

Original Article

Cuproptosis associated genes affect prognosis and tumor microenvironment infiltration characterization in lung adenocarcinoma

Xinti Sun^{1*}, Zesheng Li^{2*}, Fei Meng¹, Xingqi Huang³, Jianyao Wang¹, Jiaming Song⁴, Linao Sun¹, Peng Zhang¹

¹Department of Thoracic Surgery, Tianjin Medical University General Hospital, Tianjin, China; ²Tianjin Neurological Institute, Key Laboratory of Post-Neuroinjury Neuro-repair and Regeneration in Central Nervous System, Ministry of Education and Tianjin City, Tianjin Medical University General Hospital, Tianjin, China; ³Department of Neurosurgery, Tianjin Medical University General Hospital, Tianjin, China; ⁴Tianjin Key Laboratory of Lung Cancer Metastasis and Tumor Microenvironment, Lung Cancer Institute, Tianjin Medical University General Hospital, Tianjin, China. *Equal contributors and co-first authors.

Received June 22, 2022; Accepted September 21, 2022; Epub October 15, 2022; Published October 30, 2022

Abstract: Cuproptosis, a newly discovered mechanism of programmed cell death, is important for detailing the metabolic aspects of cancer progression and thereby guiding cancer therapy. An exciting era of translational medicine has led to the rapid development of countless immunotherapeutic strategies. The existing successful cancer immunotherapies have sparked new hope for patients with solid and hematologic malignancies. Hence, it is important to characterize the link between the cuproptosis process and the immunity status in the tumor microenvironment (TME) in Lung Adenocarcinoma (LUAD), which may be able to predict patient's prognosis. In this study, we systematically assessed 10 cuproptosis-associated genes (CAGs) and comprehensively characterized the relationship between cuproptosis and the molecular characteristics and immune cell infiltration of tumor tissue, prognosis and clinical treatment of patients. Subsequently, the CAG_score for predicting overall survival (OS) was established and its reliable predictive ability in LUAD patients was confirmed. Next, we created a highly reliable nomogram to facilitate the clinical viability of the CAG_score. The low CAG_score group, with lower immune cell infiltration, and mutation burden, had a significantly superior OS, which was associated with a better response to immunotherapy. The present study revealed that cuproptosis play a significant role in TME regulation in LUAD. Collectively, we identified a prognostic CAGs-related signature for LUAD patients. This signature may contribute to clarifying the characteristics of TME and enable the exploration of more potent immunotherapy strategies.

Keywords: Lung adenocarcinoma, cuproptosis, prognosis, tumor microenvironment, immunotherapy

Introduction

Lung cancer is one of the most malignant tumors, mainly divided into small cell lung cancer (SCLC) and non-small cell lung cancer (NSCLC) [1]. Lung adenocarcinoma (LUAD) is the principal subtype of NSCLC, accounting for 40% of all lung cancer [2, 3]. Although significant efforts have been made in early diagnosis, immunotherapy, radiotherapy, and targeted therapy, the 5-year overall survival rate of LUAD patients is still low [4-6]. The difficulty in early diagnosis, the tendency to metastasize, and molecular differences are the main causes of the bad prognosis of LUAD [7, 8]. As a result, it

is essential to develop effective therapeutic targets for LUAD and identify new biomarkers for improved diagnosis.

Programmed cell death (PCD) is an important biological process during tissue homeostasis and animal development [9]. Increasing evidence indicated that PCD including apoptosis, ferroptosis, autophagy, and others, play vital roles in tumorigenesis, progression as well as metastasis [10-12]. A study recently published in the journal *Science* is the first research to uncover cuproptosis, as a novel type of PCD, differs from ferroptosis and apoptosis in its special mechanism that excess intracellular

Cuproptosis associated genes affect LUAD

copper induces the aggregation of lipoylated dihydrolipoamide S-acetyltransferase (DLAT), which is related to the mitochondrial tricarboxylic acid (TCA) cycle, ultimately leading cell death [13]. Tsvetkov et al. revealed that copper-induced cell death requires mitochondrial respiration, but ATP from glycolysis has less effect on it. Copper does not directly participate in the electron transport chain (ETC) and only plays a role in the tricarboxylic acid (TCA) cycle. These results suggest a strong relationship between copper-induced cell death and mitochondrial metabolism, implicating a strong link between copper and the TCA cycle [13, 14]. Although the detailed mechanism underlying the role of cuproptosis in tumors is still unclear, the copper ionophore Elesclomol already helped patients whose tumors depend on mitochondria for energy. Besides, the researchers also identified 10 key genes including FDX1 involved in cuproptosis and these genes will provide direction for our subsequent analysis.

Recently, immunotherapy like immune checkpoint inhibitors (ICIs), therapeutic antibodies, and others, are gradually being widely used in the treatment of various cancers, and its effectiveness is being confirmed by more and more clinical studies [15, 16]. Although the development of ICIs like PD-1, PD-L1 as well as CTLA-4 has made great breakthroughs, only a small percentage of people benefit from it [17, 18]. Tumor microenvironment (TME) including infiltrating immune cells, tumor cells, stromal cells, and various factors have gradually been shown to be involved in tumor invasive behavior and influences tumor response to immunotherapy [19, 20]. Many studies have recently demonstrated the close link between TME and PCDs. Wang et al. found that programmed death-ligand 1 (PD-L1) blockade cause upregulation of CD8+ T cells, which release more interferon gamma (IFN γ), leading to tumor ferroptosis [21]. Liu et al. have developed the ferroptosis potential index to clarify the possible mechanism of ferroptosis in many cancers and concluded that ferroptosis is related to TME, patient survival, prognosis, and clinical treatment [22]. However, the relationship between cuproptosis, TME, and immunotherapy response in LUAD is unclear. It is necessary to dig efficient biomarkers that can divide LUAD patients into diverse groups and instruct the clinical treatment.

In this study, we analyzed 10 cuproptosis-associated genes' impact on the progression, prognosis, TME, and immunotherapy response of LUAD patients from the TCGA and GEO databases. We divided LUAD patients into different cuproptosis subgroups and explored the difference in prognostic significance, molecular characteristics, anti-tumor drug sensitivity, infiltrating immune cell intensities, and response to critical ICBs. In addition, we developed a CAG_score-based risk model that predicted the clinical outcome and the OS of LUAD patients accurately. Our goal is to better elucidate the relationship between cuproptosis and lung cancer as well as to develop a viable LUAD immunotherapy.

Methods

Data acquisition

The RNA expression data, somatic mutation data, CNV files, and clinical information of LUAD patients were obtained from TCGA database (<https://portal.gdc.cancer.gov/>). Besides, GSE-31210 dataset from GEO database (<http://www.ncbi.nlm.nih.gov/geo/>) was utilized to acquire clinical parameters and normalized gene expression data. Further removed samples missing important clinical and survival information, 736 LUAD and 59 normal samples were obtained. In total, 10 CAGs (FDX1, LIAS, LIPT1, DLD, DLAT, PDHA1, PDHB, MTF1, GLS, and CDKN2A) were acquired from the previous literature [13]. The protein-protein interaction (PPI) information was obtained by the STRING database (<https://string-db.org/>).

Consensus clustering analysis of CAGs

Consensus clustering was employed to define distinct cuproptosis-related patterns by the k-means algorithms [23]. The number and consistency of clusters were built using the consensus clustering algorithm implemented in the R package "ConsensuClusterPlus" [24]. Using gene set variation analysis (GSVA) with the KEGG gene set (c2.cp.kegg.v7.4), we identified the functional differences among subclusters according to the CAGs [25].

Relationship among molecular patterns, clinical characters, and TME

The association between molecular patterns, OS, and clinical characteristics including age,

Cuproptosis associated genes affect LUAD

gender, pathological stage, survival time, and status was investigated to determine the clinical significance of the cluster. K-M analysis was applied to evaluate the difference in OS between different patterns using R packages “survival”. Using the ESTIMATE algorithm to calculate the immune and stromal scores of LUAD patients [26]. Besides, we calculated the infiltrating of immune cells and functions based on the CIBERSORT and ssGSEA algorithm [27, 28]. We also calculated the association among the two subgroups on critical immune checkpoint genes (ICPs) expression.

Identification of DEGs between molecular patterns

We applied the “limma” R package to distinguish the differentially expressed genes (DEGs) in the cuproptosis subgroups following criteria ($|\log_2\text{-fold change (FC)}| \geq 1$, $P\text{-value} < 0.05$). Based on the DEGs, we applied GO and KEGG analysis using the R package “cluster-Profile” [29]. To screen functional pathways further, GSEA 4.2.1 software was further conducted (<http://www.gsea-msigdb.org/gsea/index.jsp>) [30].

Construction of the cuproptosis-associated prognostic CAG_score

CAG_score was established to provide a better assessment of the prognosis of LUAD patients. 739 LUAD samples were split into the training set ($n = 408$) and testing set ($n = 331$) randomly. The training set was adopted to construct the CAG_score, and the testing set and the entire set were further employed to verify the accuracy of the established risk model. Based on 486 DEGs among cuproptosis clusters, we further applied univariate Cox regression analysis to identify survival-associated genes. Ultimately, we generated CAG_scores with the following formula: $\text{CAG_score} = \text{gene expression (1)} \times \text{coefficient (1)} + \text{gene expression (2)} \times \text{coefficient (2)} + \text{gene expression (n)} \times \text{coefficient (n)}$. LUAD patients were divided into high- and low-risk groups according to the optimal cut-off value determined by the “survminer” package.

Assessment of the prognostic CAG_score and establishment of nomogram

K-M analysis was applied to compare the OS between high-risk and low-risk groups using

the R package “survival”. Principal component analysis (PCA), as well as t -distributed stochastic neighbor embedding (t -SNE) analyses, were used to lessen the dimensions and visualize the distinction between the high-risk and low-risk groups. We further applied univariate and multivariate Cox analysis to verify whether CAG_score was an independent prognostic factor using the R package “survival”. Using the R package “RMS”, we established a nomogram integrated CAG_score as well as other clinicopathological characteristics to better predict the 1-, 3-, and 5-year OS of LUAD patients. Subsequently, the predictive capability of the nomogram was evaluated by calibration curves, concordance index (C-index), and decision curve analysis (DCA). Besides, the Receiver operating characteristics (ROC) curve of 1-, 3-, and 5-year was drawn to further verify the predictive power of the established nomogram using the R package “timeROC”.

Exploration of TME and TMB between high- and low-risk groups

We explored the infiltrating of immune cells and immune functions in the high- and low-risk groups using the above methods. In addition, Wilcoxon analysis was used to compare immune cell levels and infiltrating function between the two risk groups. We analyzed tumor mutation burden (TMB) using the package “maftools” [31] and divided all LUAD patients into high- and low-TMB groups according to the median TMB score. Besides, we calculated the correlation between the risk model and TMB using Spearman correlation analysis.

Exploration of immunotherapeutic treatment

To evaluate the clinical performance of immunotherapy for LUAD patients in different risk groups, we calculated the semi-inhibitory concentrations (IC50) for common anti-tumor drugs such as cisplatin, paclitaxel, gemcitabine, gefitinib, among others, using the R package “pRRophetic” [32]. Furthermore, to identify potential drugs that can treat LUAD, we identified many promising compounds obtained from the GDSC website (<https://www.cancerrxgene.org/>) with significantly different IC50 values between the two groups. We further assessed the immunophenotype score (IPS) for LUAD patients among two subgroups. The results were downloaded from the Cancer Imaging Archive (TCIA) database (<https://tcia.at/home>).

Statistical analysis

The statistical analyses and data visualization were conducted in the R platform, GSEA software, and the string website. Student's t-tests were applied to determine the difference between the two groups. For the analysis of differences between K-M curves, the log-rank test was performed. For the above methods of analysis where no special instructions are given, $P < 0.05$ was considered statistically significant.

Results

The landscape of CAGs in LUAD

The flow chart of this study is shown in **Figure 1**. We identified the expression levels of the 10 CAGs in tumor and normal samples based on the TCGA-LUAD dataset. As shown in **Figure 2A, 2B**, the expression levels of LIAS, LIPT1, DLD, DLAT, PDHA1, PDHB, and CDKN2A were significantly upregulated in LUAD samples, whereas the expression level of MTF1 and FDX1 were downregulated in LUAD samples. Then we explored the incidence of CNVs and somatic mutations of 10 CAGs in LUAD. Additionally, the CNV alteration frequency suggested that alterations were prevalent across all 10 CAGs (**Figure 2C**). Among them, the CNV of MTF1, GLS, DLD, LIAS, and LIPT1 increased, while DLAT, FDX1, and CDKN2A exhibited an extensive decrease in CNV. Furthermore, the locations of CNV alterations for 10 CAGs on chromosomes are shown in **Figure 2D**. Additionally, 54 of 561 (9.63%) LUAD samples exhibited genetic mutations, and the results showed CDKN2A (4%) associated with the highest mutation rate, followed by DLD (1%) and PDHA1 (1%) as well as the most common variant classification was a missense mutation (**Figure 2E**). Furthermore, a protein-protein interaction (PPI) network analysis by using the string website indicated that the 10 CAGs interacted with each other and PDHB was one of the hub genes (**Figure 2F**). Based on these analyses, it indicated that CAGs may play an important role in LUAD biogenesis and progression.

Construction of cuproptosis subgroups in LUAD

In total, 739 LUAD patients from TCGA and GSE31210 datasets were included in the subsequent study to identify the potential relationship between CAGs and LUAD. The prognostic

values of 10 CAGs in LUAD patients were identified with univariate Cox regression analysis (**Figure 3A; Table S1**). Additionally, we established a network to exhibit the interactions, connections, and prognostic values of the CAGs (**Figure 3B**). Besides, based on K-M analysis, we identified most of the CAGs were highly related to the prognosis of LUAD, and the high expression of DLAT, DLD, FDX1, and PDHA1 resulted in the worse OS (**Figure S1**). Based on the results, we identified most of the CAGs were highly related to the prognosis of LUAD, which indicated the potential role of CAGs in LUAD tumorigenesis. Moreover, we conducted the consensus clustering analysis to further determine the relationship between expression patterns of CAGs and LUAD subtypes. The optimal clustering stability was found to be $K = 2$, and LUAD patients were separated into cluster A ($n = 482$) and cluster B ($n = 257$) (**Figures 3C, S2**). We further applied t-SNE analysis to confirm the brilliant cluster distribution (**Figure 3D**). According to the K-M analysis, patients in cluster A had a significantly better OS than patients in cluster B (**Figure 3E**). Finally, we compared the gene expression profiles and clinicopathological features of both clusters and significant differences were found between them with respect to CAGs expression and clinical features (**Figure 3F**).

Features of TME cell infiltration in different clusters

We applied the GSVA analysis to explore the underlying mechanism and related pathways in two clusters. The result suggested that cluster A primarily connected with multiple metastasis-related pathways, such as linoleic acid, nitrogen, alpha-linolenic acid, and ether lipid metabolism. Interestingly, cluster B is mainly involved in P53 signaling and repair-related pathways such as base excision, nucleotide excision, and mismatch (**Figure 4A; Table S2**). Furthermore, we examined the infiltrating levels of 23 human immune cells in the two clusters to identify the relationship between CAGs and the TME of LUAD by using the ssGSEA algorithm. The results indicated that infiltration of eosinophil, mast cell, plasmacytoid dendritic cell, and neutrophil was significantly higher in cluster A, while the infiltration of activated CD4 T cell, gamma delta T cell, CD56 bright natural killer cell was increased in cluster B (**Figure 4B, $P < 0.05$, Table S3**). Considering that ICIs have

Cuproptosis associated genes affect LUAD

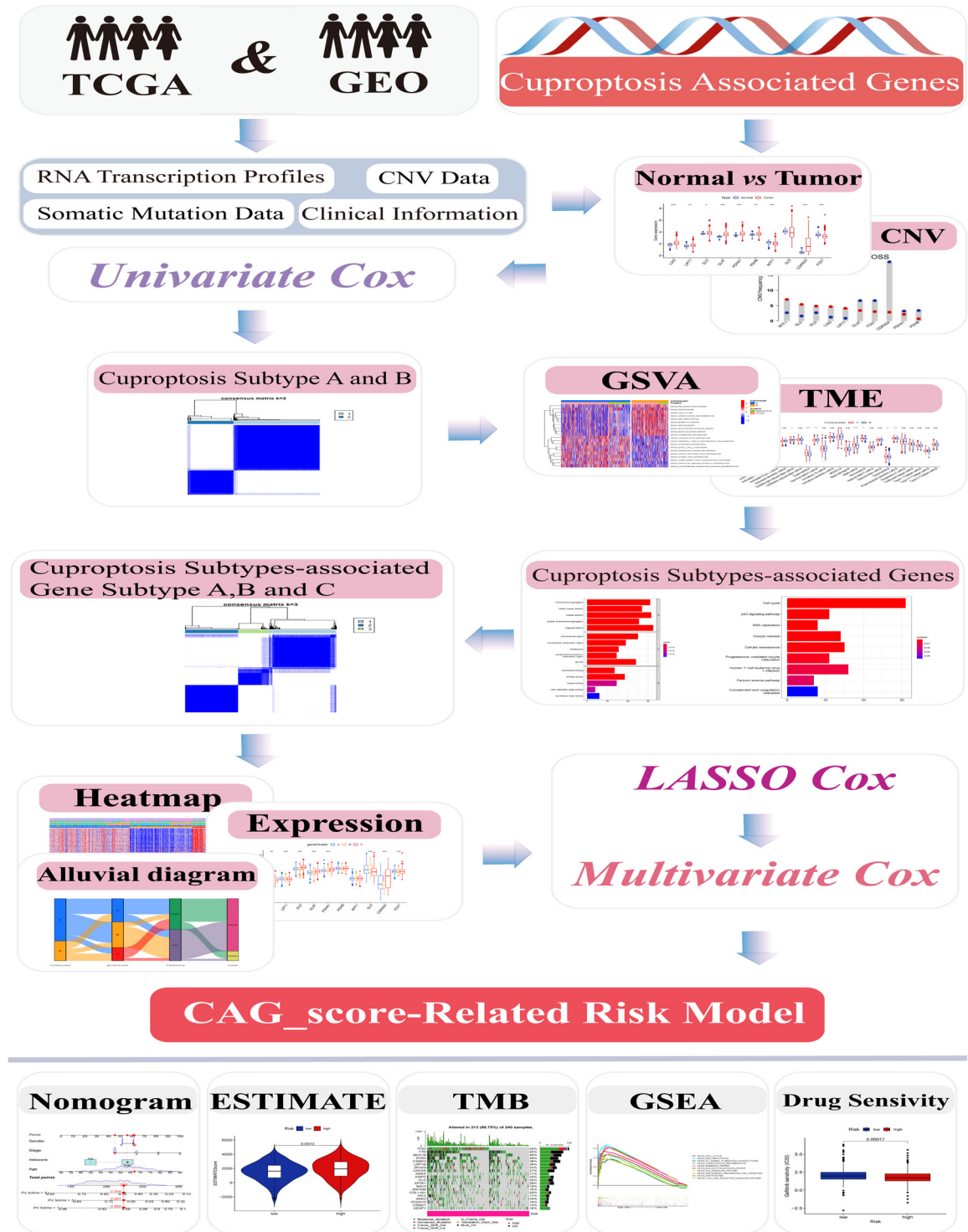


Figure 1. Flow chat.

been used for the treatment of LUAD for many years, we investigated whether there were differences in the expression of ICI-related biomarkers between the two clusters. The results suggested that cluster B correlated positively

with high PD-1, PD-L1, CTLA-4, and HAVCR2 (Figure 4C-F, $P < 0.05$). Furthermore, based on the DEGs identified between the two clusters by using the “limma” R package, we applied the GO and KEGG enrichment analyses to explore

Cuproptosis associated genes affect LUAD

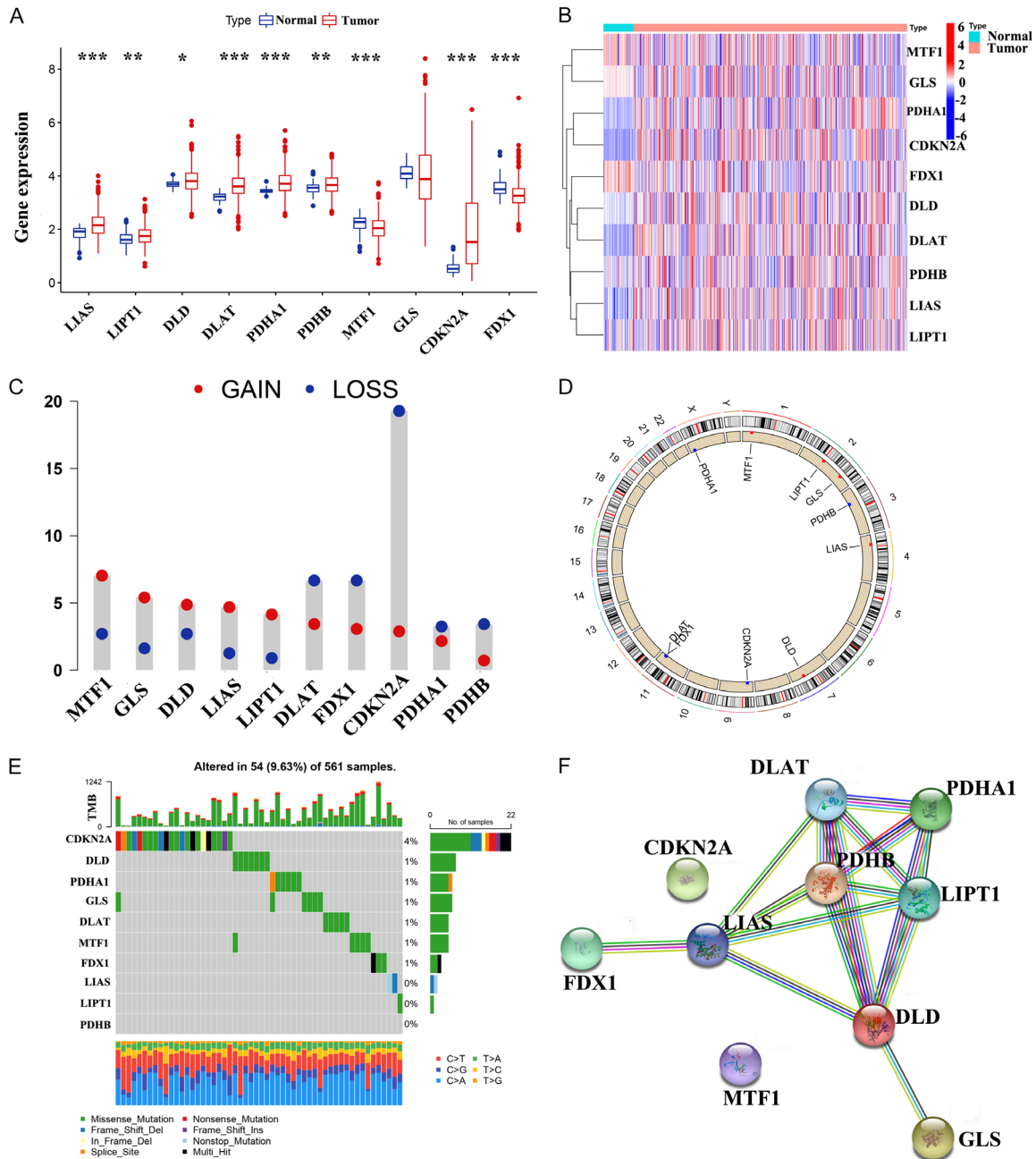


Figure 2. Analysis of expression and mutation of cuproptosis-related genes in LUAD. (A) Boxplot of 10 CAGs' expression in normal and LUAD samples. (B) Heatmap of 10 CAGs' expression in normal and LUAD samples. (C, D) The frequency (C) and chromosome distribution (D) of CNV among CAGs. (E) CAGs' mutations in LUAD. (F) CAGs form part of the PPI network. * $P < 0.5$, ** $P < 0.01$, *** $P < 0.001$, ns, no sense.

the possible enriched functions and pathways in them. GO enrichment analysis revealed that organelle fission, nuclear division, chromosomal region, and active ATPase are significantly enriched in biological processes, cell components, and molecular functions (Figure 4G; Table S4). KEGG enrichment analysis revealed that these DEGs are mainly connected with the

cell cycle, P53 signaling pathway, Cellular senescence, and other immune related pathways (Figure 4H; Table S4).

Identification of gene subgroups according to DEGs

Considering such a large prognostic difference between the two clusters, we further applied

Cuproptosis associated genes affect LUAD

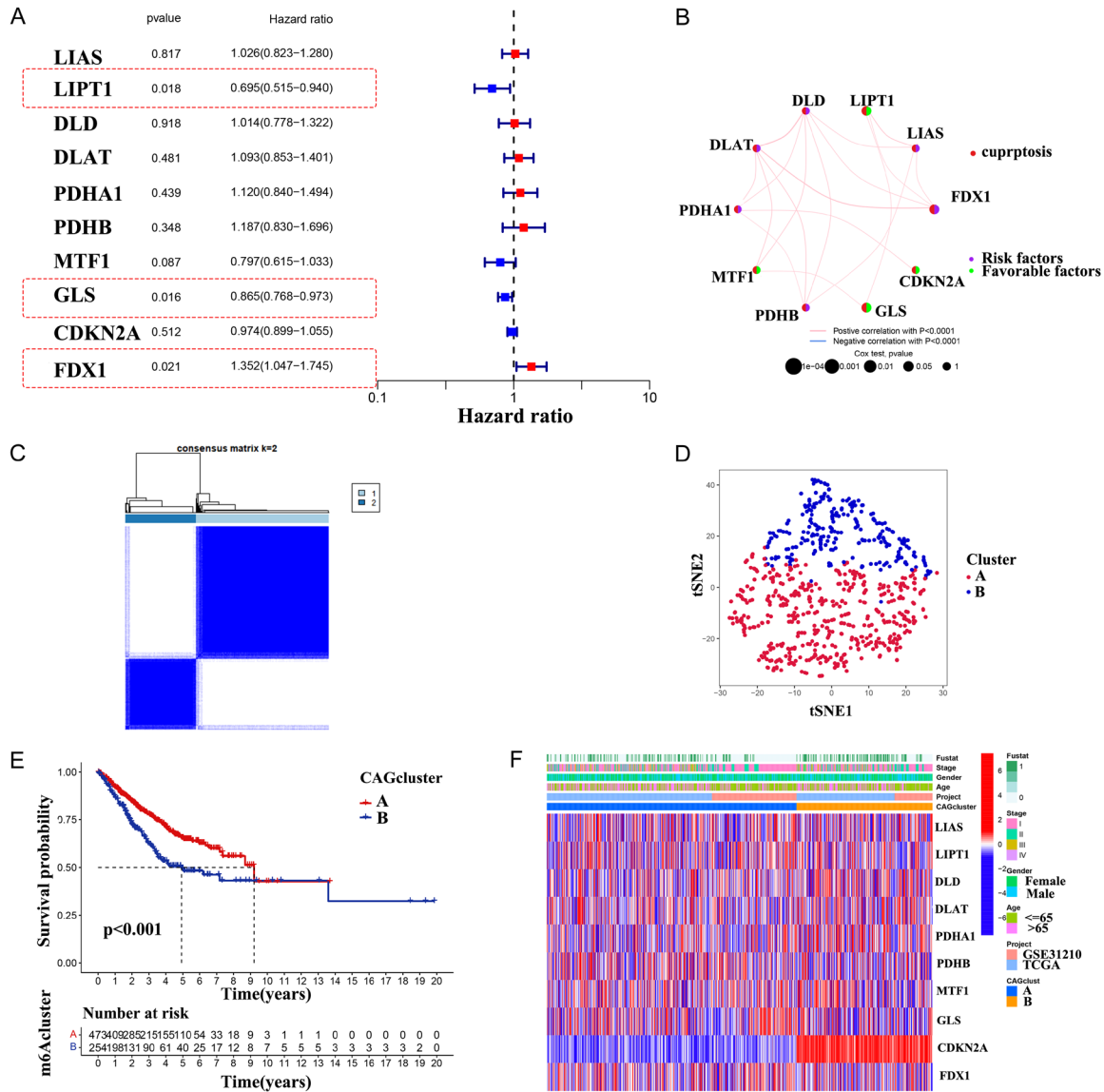


Figure 3. Differences in OS and distribution of cuproptosis-related genes between two clusters. (A) The univariate Cox Analysis for CAGs. (B) The network of correlation with CAGs in LUAD. (C) The heatmap of consensus clustering ($k = 2$) in LUAD. (D, E) Analysis of t -SNE (D) and Kaplan-Meier curve (E) among two clusters. (F) Two clusters were identified by the CAGs with a heatmap and clinicopathological profiles.

the univariate Cox regression analysis to determine the survival significance of the 468 DEGs among clusters A and B, and 393 genes were ultimately identified (Table S5). To better investigate the underlying mechanisms responsible for this differential prognosis, we used a consensus clustering approach to further differentiate patients according to 393 prognostic genes (Clusters A-C) (Figures 5A, S3). Furthermore, K-M analysis indicated that patients in cluster B had the superior OS time, whereas patients in cluster C had the shortest survival time (Figure 5B). Besides, the correlation

between clinicopathological variables, CAG clusters, and gene clusters was shown in Figure 5C. As expected from the cuproptosis clusters, the cuproptosis gene clusters proved the significant discrepancies in CAGs' expression (Figure 5D).

Construction and validation of the CAG_score related risk model

The CAG-score related risk model was established according to the CAG cluster-associated DEGs. The training set was employed to con-

Cuproptosis associated genes affect LUAD

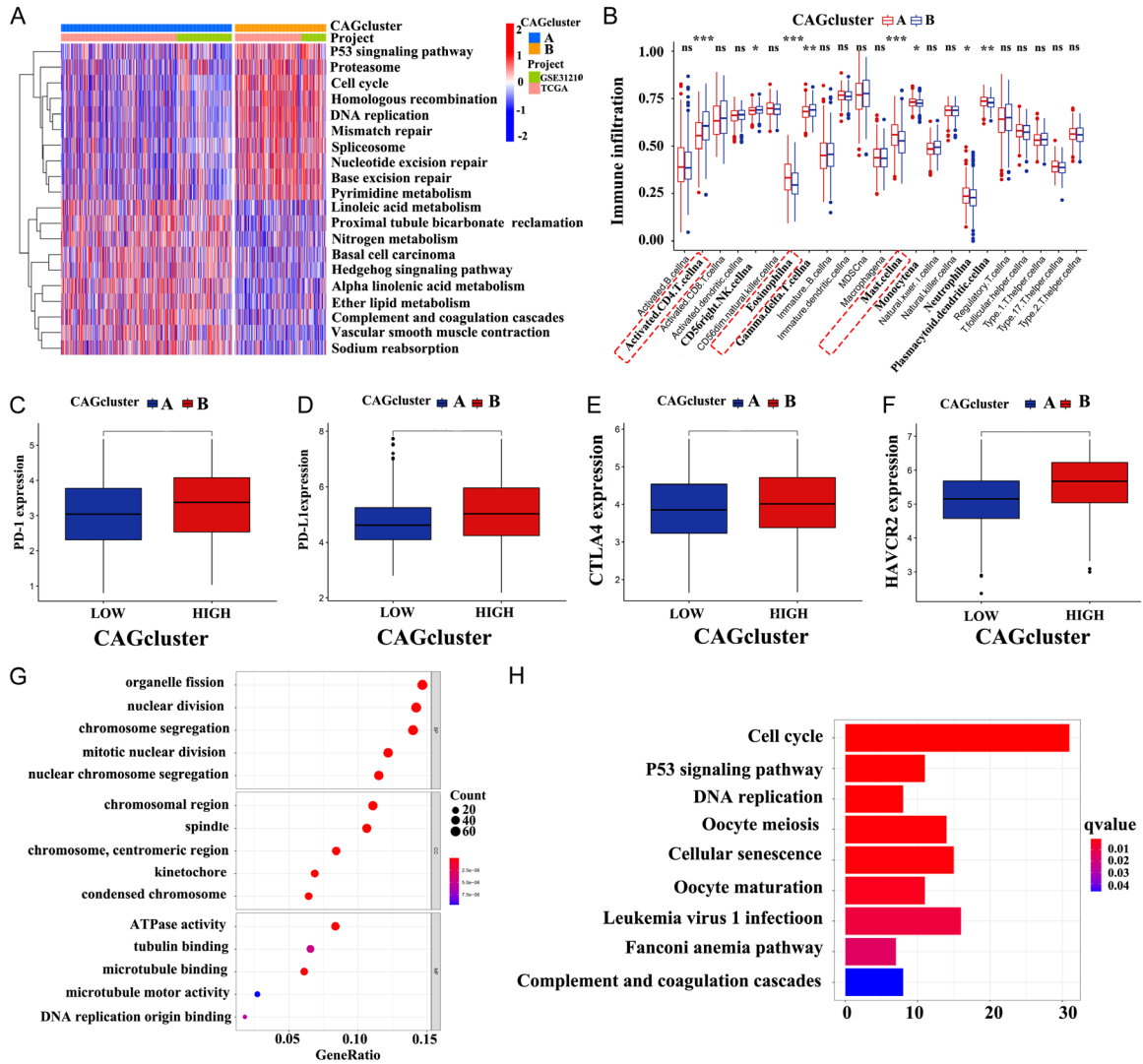


Figure 4. Exploration of the role of immune checkpoints and differentially expressed genes. (A) GSEA between two clusters in TCGA and GSE31210. (B) The infiltration level of 23 immune cell types in two clusters. (C-F) Expression of PD-1 (C), PD-L1 (D), CTLA-4 (E), and HAVCR2 (F) between two clusters. (G, H) GO (G) and KEGG (H) analyses for biological functions and pathways. * $P < 0.5$, ** $P < 0.01$, *** $P < 0.001$, ns, no sense.

struct the CAG-score related risk model; meanwhile, the testing and entire set were applied to assess the predicted ability of the established model. LASSO and multivariate Cox regression analysis for 393 cuproptosis cluster-associated prognostic DEGs were further conducted to identify and establish an optimal risk model. Finally, we obtained two genes including CD55 and SPP1. Then we calculated the CAG_score with the following formula: $CAG_score = (-1.21914109097502 \times \text{expression of CD55}) + (0.574745465004888 \times \text{expression of SPP1})$. LUAD patients were divided into high- and low-risk groups according to the optimal cut-off

value determined by the “survminer” package. Furthermore, we explored the distribution of samples and correlation among the two cuproptosis clusters, three gene clusters, and two groups (high-risk group and low-risk group) (Figure 6A). Additionally, we observed a significant difference between the cuproptosis clusters and gene clusters in the CAG_score (Figure 6B, 6C). Based on the abovementioned survival analysis, we identified that higher CAG_scores of both classifications were correlated with worse survival. Besides, K-M analysis also indicated that LUAD patients in the high-risk group had a worse OS than in the low-risk group

Cuproptosis associated genes affect LUAD

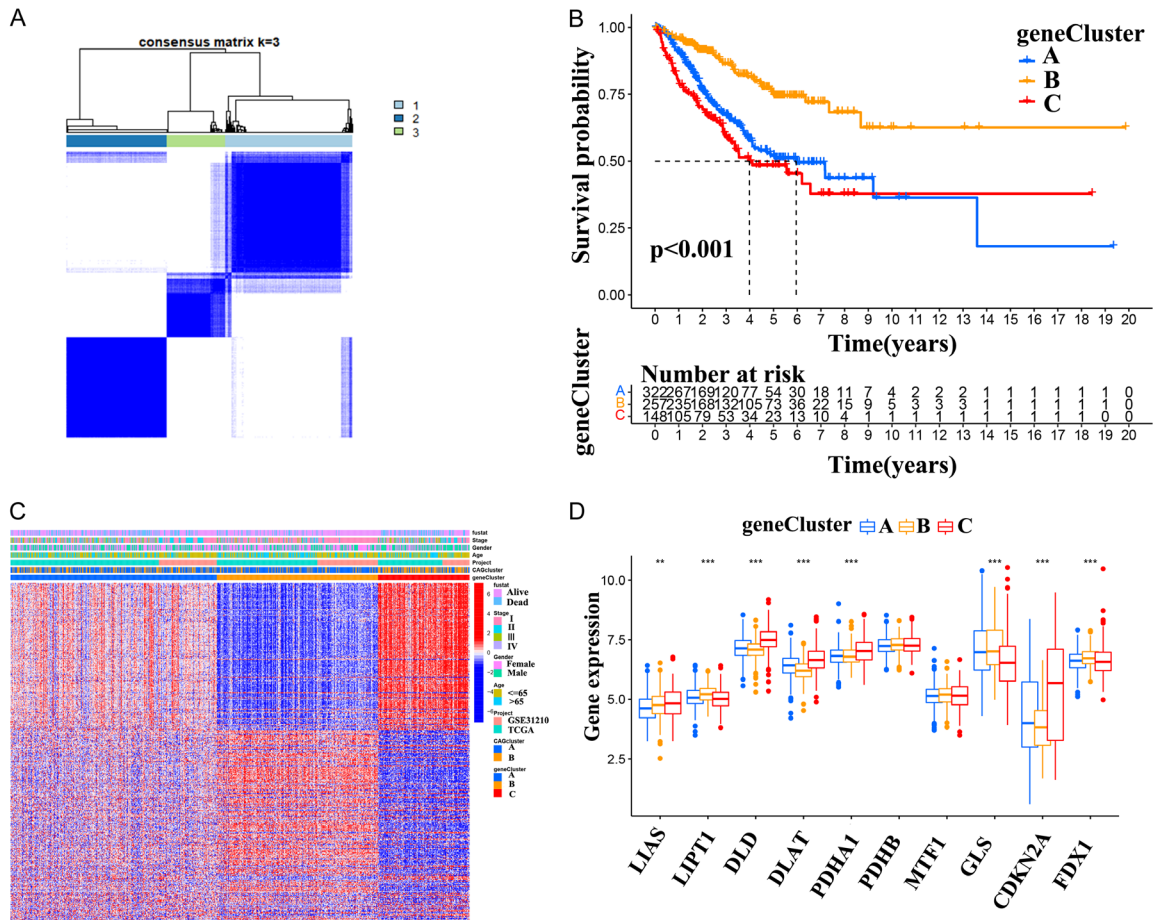


Figure 5. Identification of gene subgroups. A. 3 matrices from consensus clustering. B. Survival analysis of three gene subgroups in LUAD. C. Heatmap and clinicopathological features between three gene subgroups. D. The expression level of CAGs in three gene subgroups. * $P < 0.05$, ** $P < 0.01$, *** $P < 0.001$, ns, no sense.

(Figure 6D, $P < 0.05$). Subsequently, the C-index analysis was used to evaluate the model's prediction capability, and CAG_score has a higher c-index than other clinical traits (Figure 6E). In addition, the distribution of CAG_scores and survival status among patients in two groups suggested an association between increased CAG_scores and decreased OS (Figure 6F, 6G). The relative expression standards of the two genes for every patient were shown in Figure 6H. We further used PCA and *t*-SNE analysis to assess the distribution among the two subgroups and clear distribution results demonstrate the accuracy of our model, subsequently (Figure 6I, 6J).

Assessment of the CAGs-related risk model

To determine the prognostic capability of the established model, CAG_score for LUAD patients in the testing and entire set were calcu-

lated using the above formula. Similarly, K-M analysis suggested a better OS of patients in low-risk group among testing and entire sets (Figure 7A, 7B). The distribution of risk scores, as well as the survival status of patients in the testing and entire sets, was displayed in Figure 7C-F. Furthermore, the relative expression standards of the two genes for LUAD patients among testing and entire sets were also shown in Figure 7G, 7H. PCA and *t*-SNE analyses were applied to evaluate the accuracy of the risk model based on testing (Figure 7I, 7J) and entire sets (Figure 7K, 7L). All the above bioinformatics studies manifested that the established risk model according to CAG_score was accurate and promising.

Independent prognostic value of the CAG_score and construction of nomogram

To determine whether CAG_score was an independent prognostic factor for OS among LUAD

Cuproptosis associated genes affect LUAD

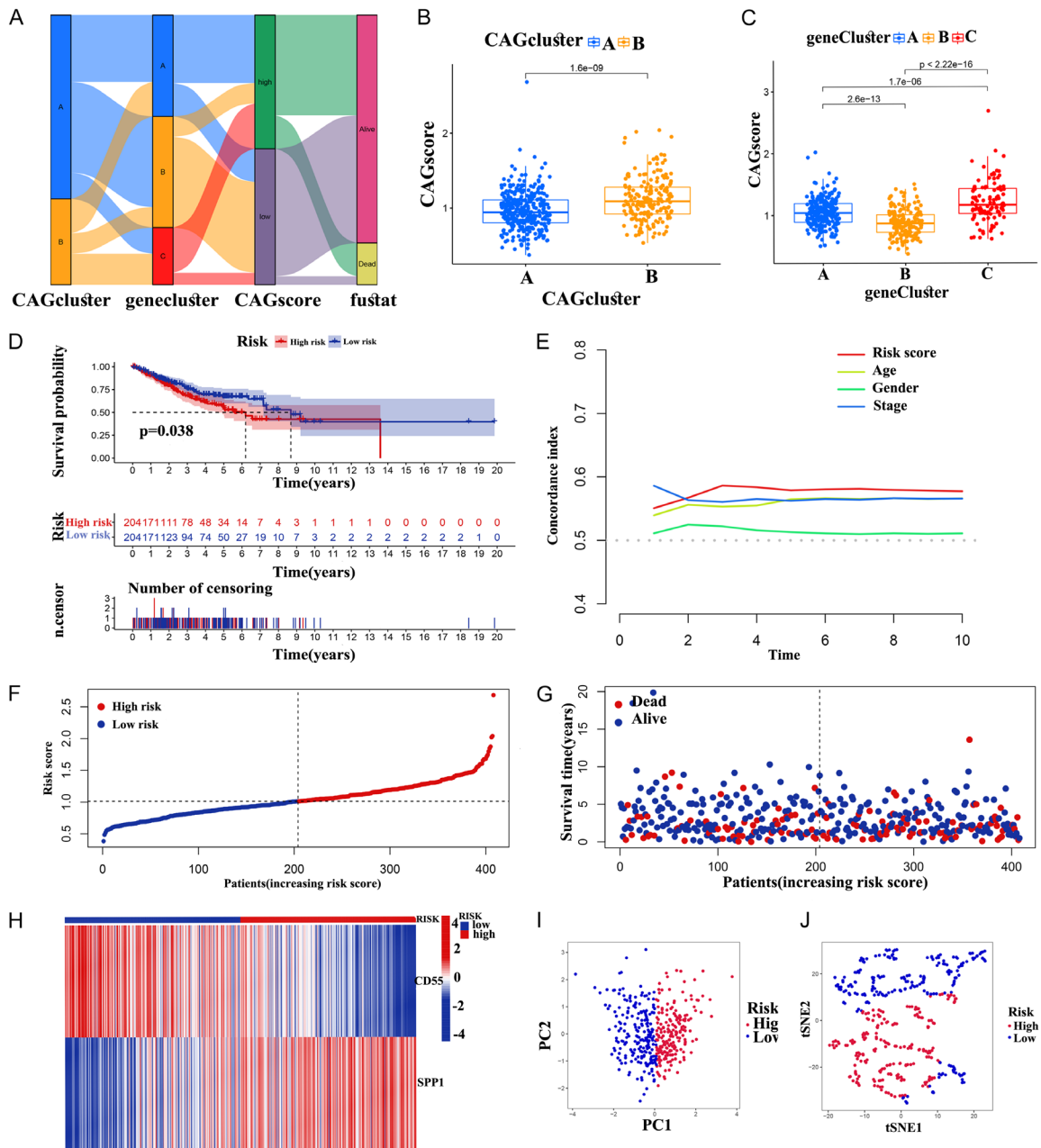


Figure 6. Construction of the model based on the CAG score. (A) Alluvial diagram of inner Connections between CAG cluster, gene cluster, CAG score, and survival status. (B, C) The difference in CAG score among CAG cluster (B) and gene cluster (C). (D) The distinction of OS between high- and low-risk groups. (E) Predictive capability evaluation in the concordance index. (F-I) Distribution types of risk levels (F), living status (G), expression of prognostic signatures (H), PCA (I) and t-SNE (J) analyses in the training set.

patients, we carried out the univariate and multivariate Cox analyses. According to the univariate regression assessment, the hazard (HR) of CAG_score and the 95% confidence interval (CI) were found to be 2.511 and 1.585-3.980 (Figure 8B, $P < 0.001$). Furthermore, after adjusting for other confounding factors, multi-

variate regression analysis presented that the CAG_score still has a statistically significant effect on OS (HR = 2.295, 95% CI = 1.434-3.673) (Figure 8A, $P < 0.001$). Based on the above results, it is concluded that the risk prognostic model according to CAG_score serves as independent prognostic factor for LUAD

Cuproptosis associated genes affect LUAD

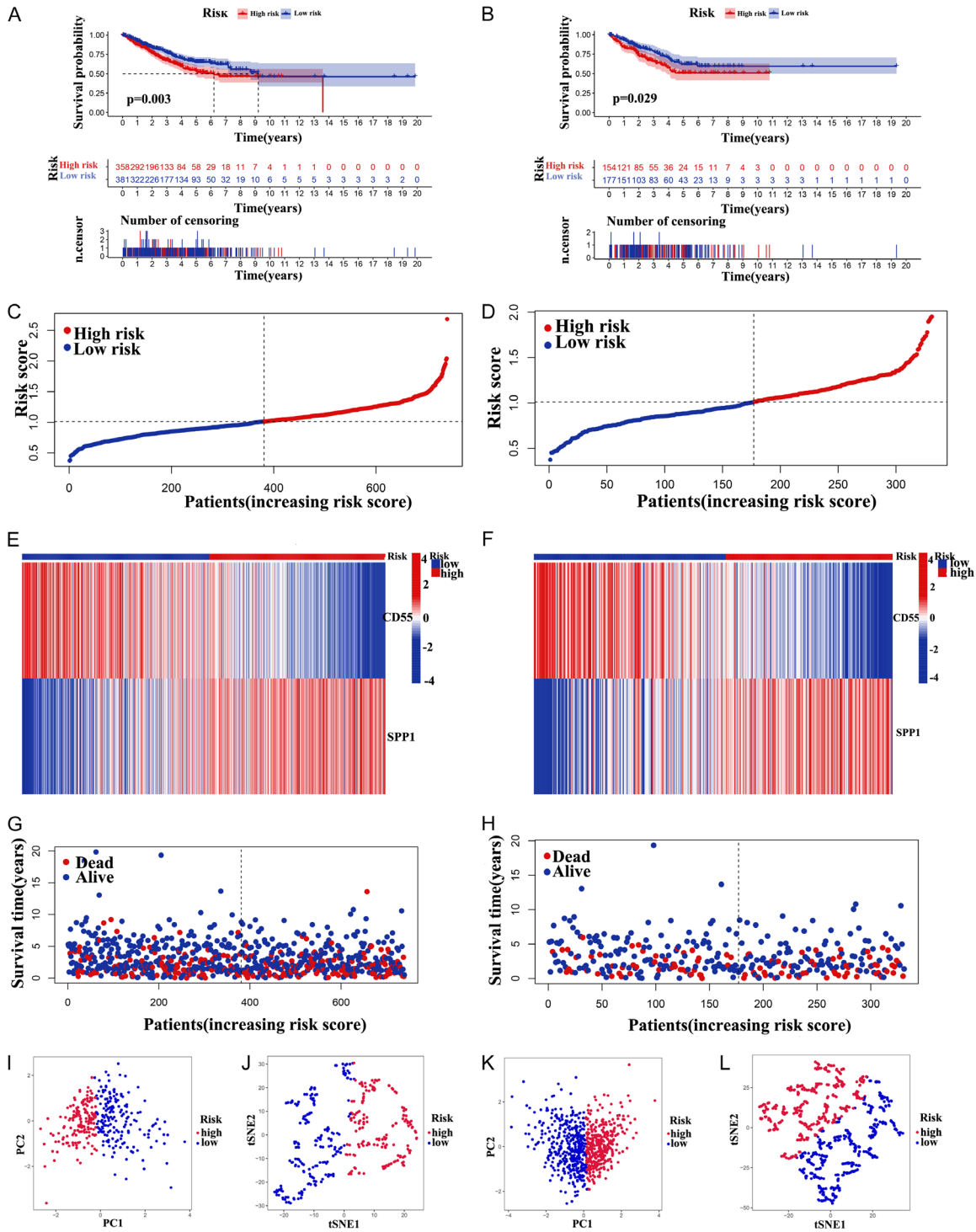


Figure 7. Validation of the CAG score model based on the testing and entire sets. (A, B) K-M analyses based on the testing set (A), and the entire set (B). (C, D) Distribution of CAG scores based on the testing set (C), and entire set (D). (E, F) Relative expression of 2 hub genes based on the testing set (E), and the entire set (F). (G, H) Survival status and survival time patterns are based on the testing set (G), and the entire set (H). (I-L) PCA and t-SNE analyses between the high-risk and low-risk groups based on the testing set (I, J) and entire set (K, L).

patients. Additionally, we established a nomogram that takes into account gender, age,

stage, and CAG_score to better predict survival for LUAD patients at 1-, 3-, and 5-years (Figure

Cuproptosis associated genes affect LUAD

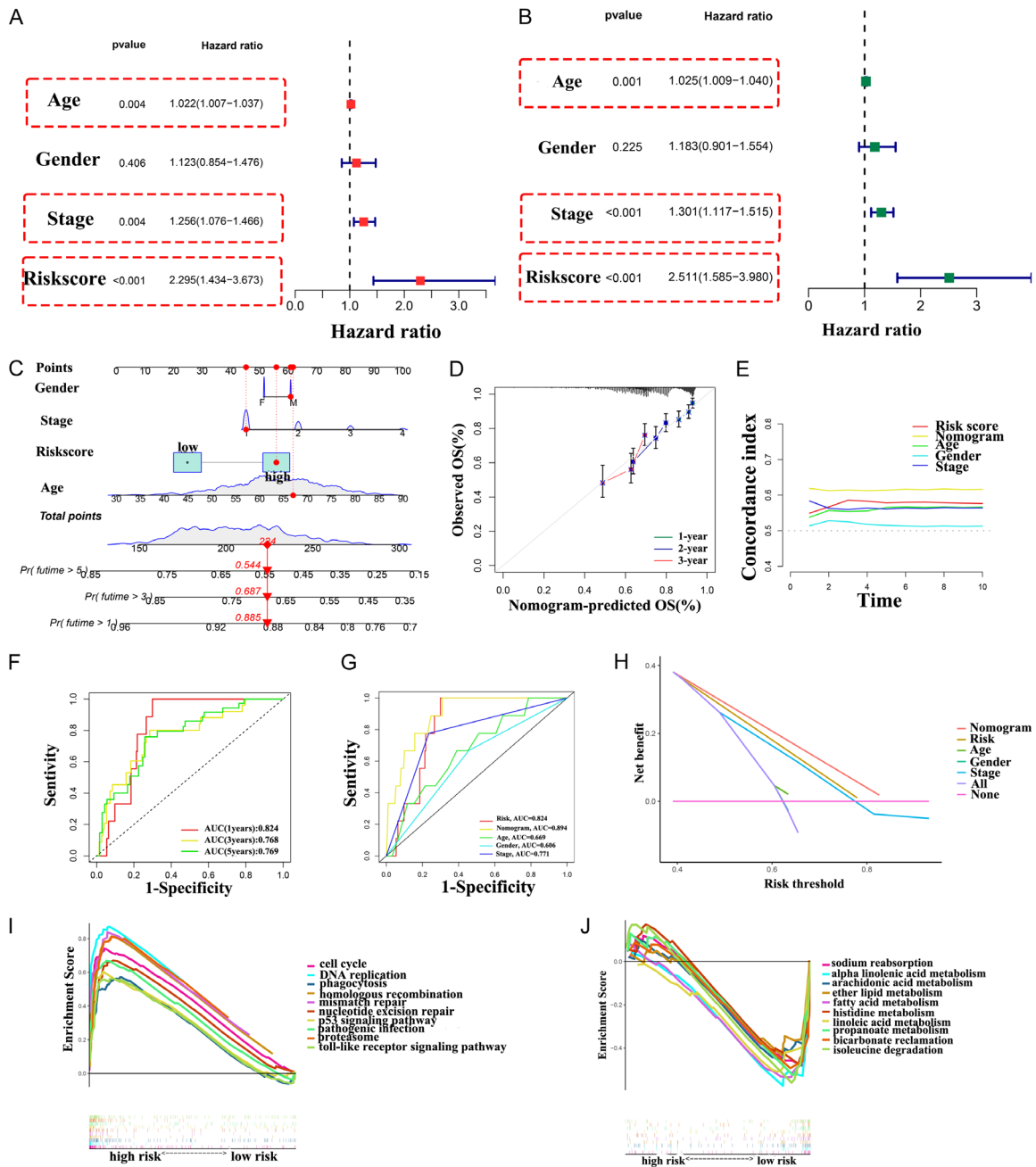


Figure 8. Development and assessment of the nomogram. (A, B) Multivariate (A) and univariate (B) Cox analyses based on the entire set, respectively. (C) The nomogram. (D) The calibration curves of the nomogram predict the probability of the OS (The x-axis shows nomogram-predicted survival, and the y-axis shows actual survival. The grey line shows the ideal calibration line, and the color line represents the model-predicted calibration line). (E) The concordance index of the nomogram, CAG_score (risk score), and clinical characteristics. (F) ROC curves for 1-, 3-, and 5-year OS in the nomogram. (G) OS comparison in ROC curves for clinical characteristics, CAG_score, and the nomogram. (H) Evaluation of clinical applicability of the nomogram with DCA curves. (I, J) The exploration of biological pathways based on GSEA in the high- (I) and low-risk (J) groups.

8C). The accuracy of the nomogram was verified in subsequent calibration curves, and we found a high degree of accuracy between the actual observed and predicted values (**Figure**

8D). Besides, compared with other clinical indicators, the nomogram showed the highest C-index (**Figure 8E**). Besides, the area under the ROC curve (AUCs) at 1, 3, 5-year were

0.824, 0.768, and 0.769, suggesting that the nomogram was reliable in predicting the OS of LUAD patients (**Figure 8F**). In addition, we analyzed the AUCs of the risk model and other clinical factors to further test the accuracy and sensitivity of the risk model. The nomogram's AUCs for predicting 1-, 3-, and 5-year survival were higher than those for other clinical factors (**Figure 8G**). The DCA curves also confirmed the superior predictive power of the nomogram (**Figure 8H**). For a deeper exploration of the mechanisms that contribute to significant differences between two groups in the multidimensional analysis, we performed the enrichment analysis using GSEA software. In the results, it was evident that the high CAG_score group was enriched in the pathway such as cell cycle, DNA replication, homologous recombination, P53 signaling pathway, and others (**Figure 8I**; [Table S6](#)), while pathways such as arachidonic acid metabolism, fatty acid metabolism, and sodium reabsorption were significantly enriched in the low CAG_score group (**Figure 8J**; [Table S6](#)).

Evaluation of immune infiltration landscape among high- and low-risk groups

Next, we applied the CIBERSORT algorithm to explore the differences in the composition of TME-infiltration cells between high- and low-risk groups ([Table S7](#)). The relative fraction of 22 immune cells within low- and high-risk groups was presented by the heatmap (**Figure 9A**), and the box plot (**Figure 9B**). The results showed significant differences in the distribution of immune cells based on risk model. We further conducted the ssGSEA algorithm to explore the difference of immune cell infiltration and immune response for LUAD patients among high-risk and low-risk groups ([Table S8](#)). The results of immune cell infiltration suggested that infiltration of Macrophages, Treg, NK cells, and T helper cells were obviously increased in the high-risk group (**Figure 9C**). Similarly, the immune functions such as APC co-inhibition, stimulation, CCR, Check-point, MHC-class-I, and T cell co-inhibition were significantly higher in the high-risk group (**Figure 9D**). Additionally, we applied the ESTIMATE algorithm to analyze the immune, stromal, and estimate scores of LUAD patients. It was found that LUAD patients in the high-risk group had a significantly higher immune score, stromal

score, and estimate score than in the low-risk group (**Figure 9E-G**, $P < 0.05$). We also identified the relationship between CAG_score and TME scores, and the results suggested that the immune score, stromal score, and estimate score were positively correlated with CAG_score (**Figure 9H-J**). In order to assess the correlation between the CAG_score and immune cell subtype infiltration, we conducted a comprehensive analysis using multiple immune-related algorithms including TIMER, CIBERSORT, xCELL, quanTIseq, MCPcounter, EPIC, and CIBERSORT-ABS. The results indicated that there was a positive relationship between immune cell infiltration and CAG_score (**Figure 9K**). We then investigated the correlation between CAG_score and immune cells, and we found that most immune cells were highly correlated with both genes (**Figure 9L**). According to the findings above, high-risk patients tended to have a high immune infiltration status, which may be responsible for the poor prognosis.

Difference between clinical characteristics and TMB among subgroups

Considering the significant differences between high-risk and low-risk groups, we further explored the relationship between CAG_score and different clinical characteristics. The results suggested that no significant distributional difference was found with respect to age ($\leq 65 / > 65$ years) ($P > 0.05$, **Figure 10A**), stage I, III, and IV ($P > 0.05$, **Figure 10B**), Myc expression ($P > 0.05$, **Figure 10C**). Interestingly, clinical differences were found in terms of stage I and stage II ($P = 0.00039$, **Figure 10B**), ever smoking and never smoking ($P = 0.0018$, **Figure 10D**), gender ($P = 0.036$, **Figure 10E**), ALK fusion + and EGFR mutation + ($P = 0.006$, **Figure 10F**) and other alteration status. In addition, as TMB emerged as an important predictor of tumor immune response, we examined TMB differences between high- and low-risk groups in more depth. The results demonstrated that the high-risk group had a significantly higher TMB status ($P = 0.028$, **Figure 10G**). The CAG score and TMB exhibited low linear correlation ($R = 0.095$, $P = 0.034$, **Figure 10H**). Based on the median cut-off of TMB scores, we divided LUAD patients into high and low TMB groups. Furthermore, we applied K-M analysis to investigate the impact of TMB status on prognosis in LUAD patients. The results suggested that high-

Cuproptosis associated genes affect LUAD

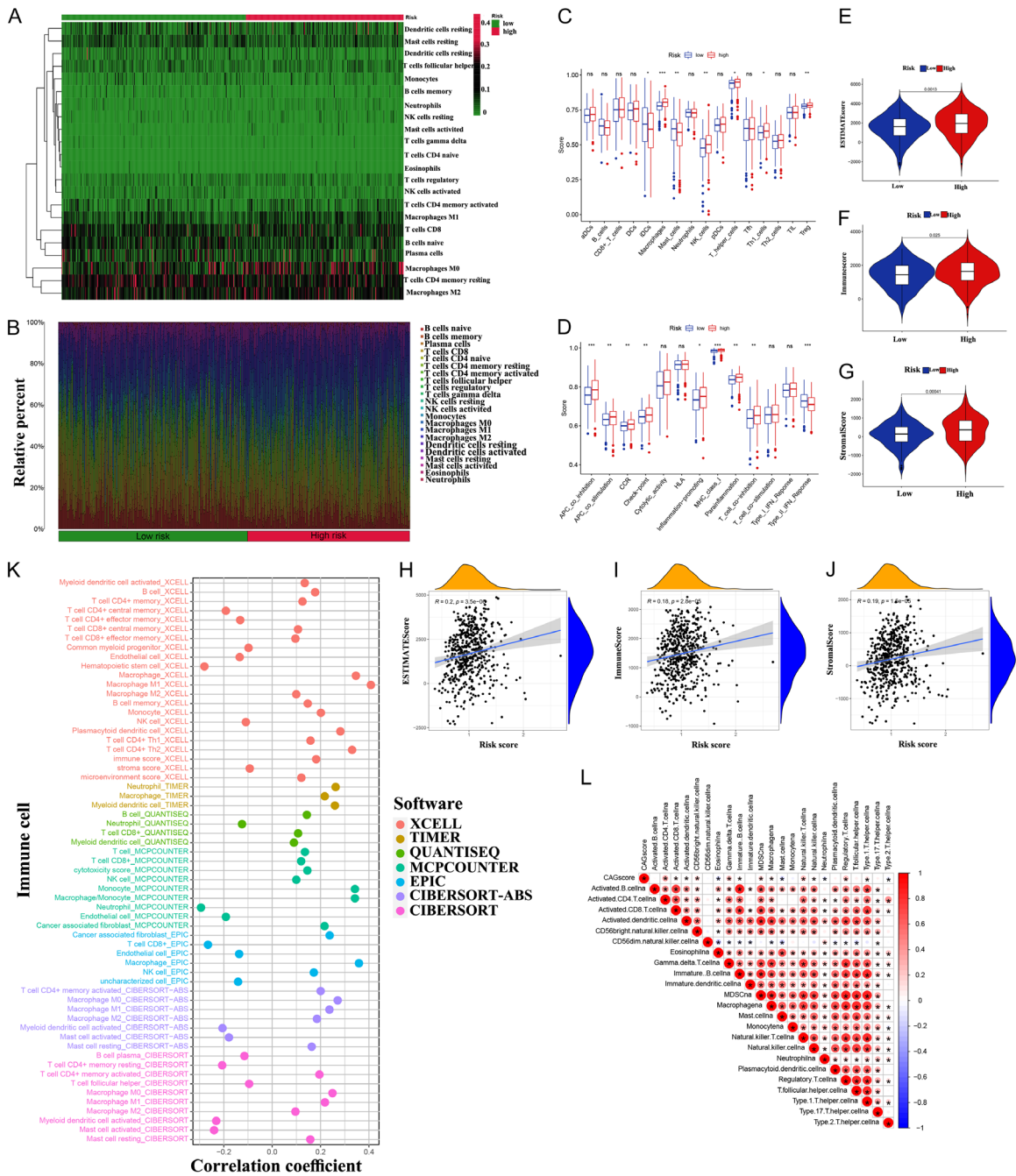


Figure 9. Characterization of immune cells infiltration in TME. (A, B) Expression features of 22 immune cells in the heatmap (A), and the box plot (B) using the CIBERSORT algorithm. (C, D) The infiltration of immune cells (C) and immune functions (D) among high- and low-risk groups using ssGSEA algorithm. (E-G) ESTIMATE assessed sample tumor purity with the estimate (E), immune (F), and stromal (G) scores. (H-J) The relationships between the estimate (H), immune (I), stromal (J) scores and CAG_score. (K) Relationship between the CAG_score and immune cells infiltration. (L) Analysis of the correlation between the CAG_score and 23 immune cells. * $P < 0.5$, ** $P < 0.01$, *** $P < 0.001$, ns, no sense.

TMB patients had a better prognosis than low-TMB patients (Figure 10I, $P < 0.05$). Using the TMB score to predict the survival of LUAD patients or using the risk model to predict the

prognosis of patients, which one had the better predictive ability? Interestingly, when we combined the TMB and risk scores for K-M analysis of LUAD patients, we found that better OS with

Cuproptosis associated genes affect LUAD

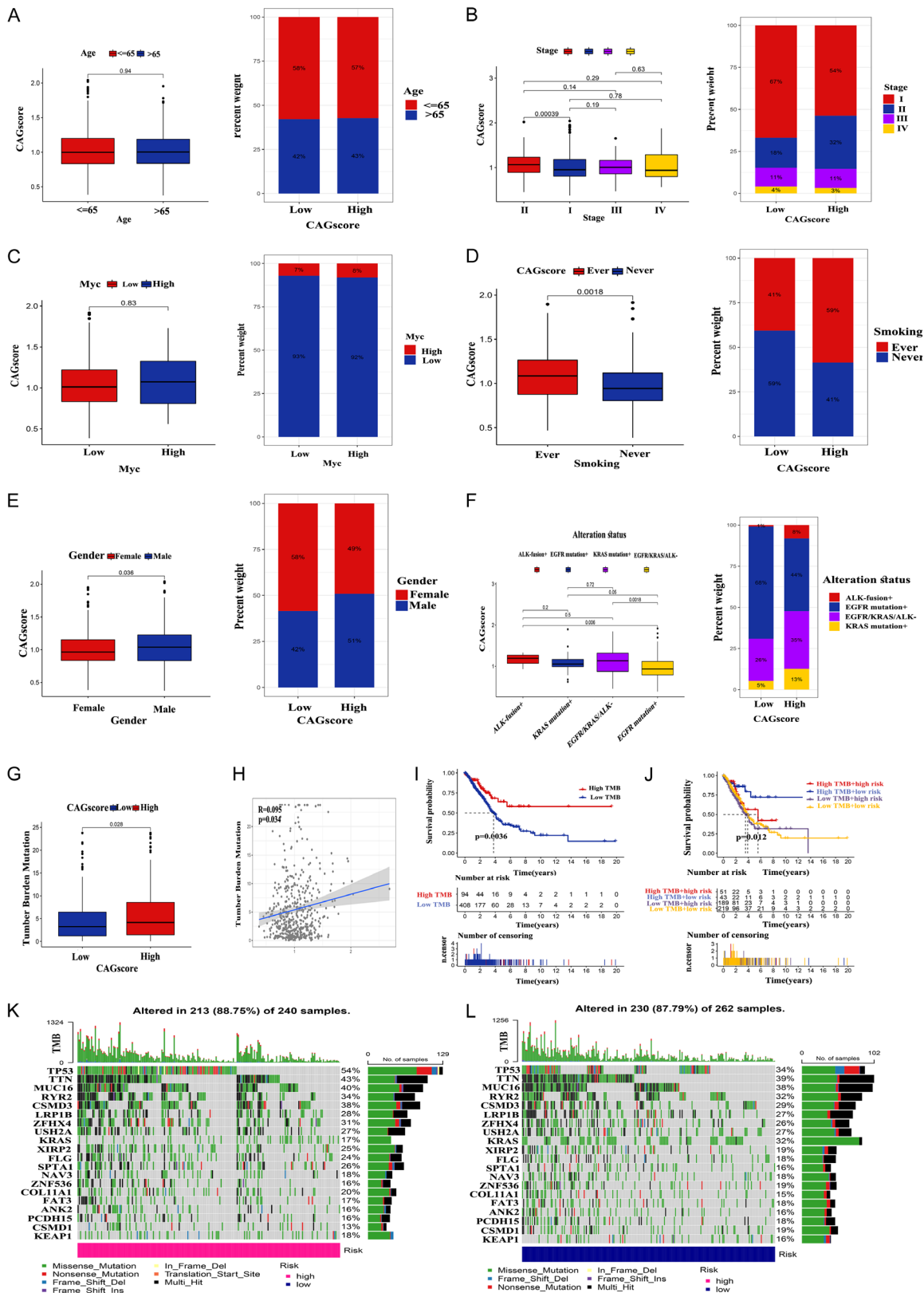


Figure 10. Comprehensive analysis of the CAG score in LUAD. (A-F) The distribution and composition of Age (A), Stage (B), Myc expression (C), Smoking history (D), Gender (E), and Alteration status (F) in LUAD. (G) The level of TMB between high- and low-risk groups. (H) Correlation analysis of the CAG score and TMB. (I, J) K-M analysis the OS between the low- and high-TMB groups (I), and four groups stratified by both TMB and CAG_score (J). (K, L) Somatic mutation landscape in the high- (K) and low-risk (L) groups.

high-TMB was eliminated by the risk score. On the contrary, the patients in the group (low-risk score and high TMB score) had a significantly better OS than in the other groups, and it could be concluded that the CAG_score risk model was superior to the TMB in predicting an individual's prognosis (**Figure 10J**). Based on the TCGA-LUAD dataset, we also examined whether there were differences in the distribution of somatic mutations between high-risk and low-risk patients. The top 20 driver genes including TP53, TTN, MUC16, RYR2, CSMD3, and others among two subgroups were displayed in **Figure 10K, 10L**.

Clinical treatment and drug sensitivity analysis

As the prognosis of low-risk and high-risk patients differs greatly, we anticipate different responses to immune drugs and immune checkpoints among patients in different risk groups. We calculated IPS scores to detect the immune response-ability of LUAD patients. According to the results, patients in the low-risk group had a greater IPS score, suggesting that low CAG_score patients may be more responsive to immunotherapy (**Figure 11A**). Additionally, to identify the potency of the CAG score as a biomarker to predict therapeutic response in LUAD patients, we further applied the "pRRophetic" package to appraise the IC50 values of 138 drugs available in the Genomics of Drug Sensitivity in Cancer (GDSC) database. The IC50 of AZD.0530, AUY922, ATRA, AP.24534, AMG.706, AKT inhibitor VIII, AICAR, ABT.263, and A.443654 were significantly higher in the low-risk groups, indicating that high CAG_score patients might benefit from these drugs (**Figure 11B**, $P < 0.05$). Furthermore, we calculated the IC50 of common antitumor drugs treated for lung cancer among two subgroups and found that low-risk patients had a higher IC50 for chemotherapeutics such as cisplatin, paclitaxel, gemcitabine and target therapy such as gefitinib and erlotinib, suggesting that CAG_score served as a promising predictor of anti-tumor drug sensitivity (**Figure 11C**, $P < 0.05$). Furthermore, we investigated the expression of ICPs between patients with different risk groups, and the results showed that the expression of most ICPs in the high-risk group was generally higher than that in the low-risk group (**Figure 11D**, $P < 0.05$).

Discussion

Cuproptosis, a new form of programmed cell death, was first revealed in journal of *Science* [13]. Different from previously reported programmed cell death including apoptosis, pyroptosis, necroptosis, and ferroptosis, excess intracellular copper induces proteotoxic stress by affecting the mitochondrial tricarboxylic acid (TCA) cycle leading to cell death [33]. There have been many studies confirming that PCD plays an important role in regulating cancer growth, immunotherapy as well as TME [10, 12, 34]. For example, the low expression of GSDMD, as the key pyroptosis affecting protein, results in the proliferation of gastric cancer cells through ERK1/2, STAT3, and PI3K/AKT pathways [35, 36]. By using bioinformatics, Wu et al. identified a large number of genes involved in ferroptosis pathways that are highly expressed in various cancers [37]. Che et al. found that mutations in ROS-induced oxidative stress pathways-related regulatory genes which as the core of ferroptosis are widely present in various cancers [38]. Additionally, autophagy has been characterized as having a dual role, whereby it can either prevent or facilitate cancer metastasis by decreasing tumor necrosis caused by hypoxia and preventing the infiltration of inflammatory cells [39, 40]. However, the exact mechanism that whether cuproptosis involved in cancer progression is unclear. Despite failed clinical trials of copper ionophores such as Elesclomol as cancer treatments, Tsvetkov et al. confirmed it already helped patients whose tumors depend on mitochondria for energy. Furthermore, now that researchers have discovered the key regulators of cuproptosis, they think copper ionophores could potentially be used to treat a range of cancers that are particularly susceptible to this process, such as cancers that overexpress the FDX1 gene [13, 41]. It needs to be specified that the biological functions and mechanism by which cuproptosis affect LUAD and TME were previously unknown. Therefore, the comprehensive role of cuproptosis-associated genes in LUAD and TME was examined in this research.

In this study, we obtained the LUAD samples by integrating the TCGA and GEO databases. Firstly, we found that the expression of CAGs was differently expressed in LUAD and normal samples as well as associated with prognosis.

Cuproptosis associated genes affect LUAD

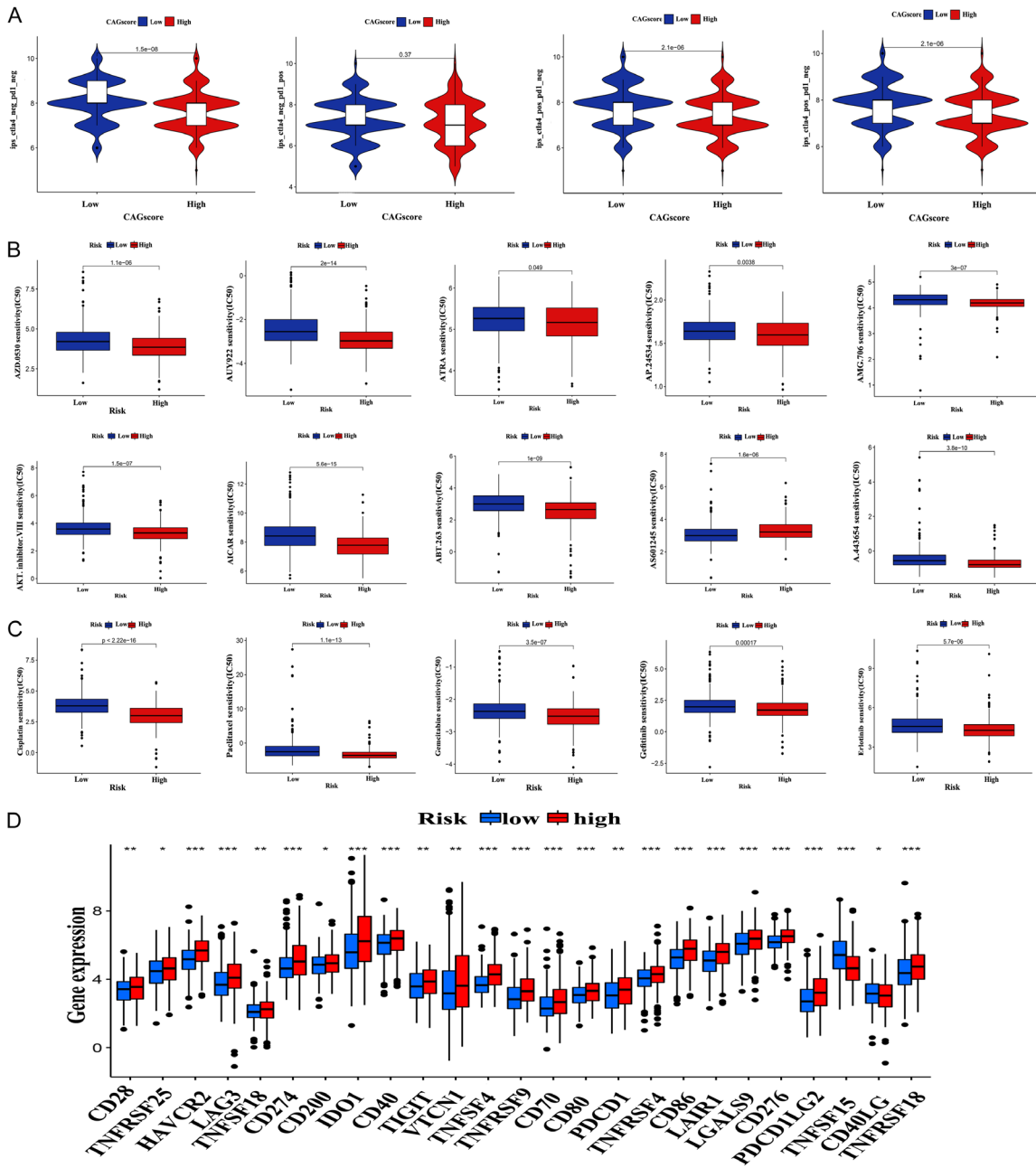


Figure 11. Sensitivity analysis of immunotherapy and chemotherapy. A. IPI score between high- and low-risk groups. B. The immunotherapy prediction of high-risk and low-risk groups. C. Drug sensitivity analysis of common chemotherapeutic drugs. D. Relationships between immune checkpoints and CAG score. * $P < 0.5$, ** $P < 0.01$, *** $P < 0.001$, ns, no sense.

Then, we divided LUAD patients into two cuproptosis clusters (clusters A and B) with different prognoses, immune infiltrations, and functions by using unsupervised clustering analysis. Furthermore, GSEA enrichment analysis indicated that cluster B was mainly enriched in carcinogenic pathways such as P53 and repair pathways such as mismatch and nucleotide

repair; and cluster A was significantly related to carcinogenic pathways and metabolism pathways. Additionally, GO and KEGG functional enrichment analyses have shown that DEGs between two clusters were highly correlated with biological processes, as well as pathways such as cell cycle, P53, ATPase activity, and organelle fission. Based on the DEGs associat-

Cuproptosis associated genes affect LUAD

ed with the subgroup signature, three gene clusters with different clinical characteristics, immune functions, and environmental effects were identified for LUAD. By using univariate and multivariate Cox regression analysis, CAG_score was established to quantify the high-risk and low-risk subgroups. The cluster B and gene cluster C with the poorest OS had the higher CAG_score in CAG_clusters as well as three gene clusters. Interestingly, high CAG_score patients had worse clinical outcomes, revealing that a high CAG_score could predict a poor prognosis. Furthermore, our functional enrichment analyses indicated that cancer- and metastasis-related pathways were significantly enriched, implying that cuproptosis may involve in the malignant behavior of LUAD.

Additionally, univariate and multivariate Cox analyses indicated that CAG_score was an independent factor for predicting LUAD patients' survival outcomes. Besides, ROCs and C-index analyses validated its predictive robustness for 1-, 3-, and 5-year OS. Therefore, CAG_score might be a reliable predictive value for the prognosis of patients. Furthermore, our results indicated that there was a significant discrepancy in TMB and somatic mutations among high and low CAG_scores. Higher TMB has been validated to be related to a better prognosis for LUAD patients, consistent with our findings [42]. Furthermore, the survival probability in the group (low CAG_score and high TMB) was significantly better than the group (high CAG_score and high TMB), suggesting CAG_score could be adopted to independently predict the responsiveness of immunotherapy.

Interactions of the immune system are critical features of tumorigenesis and serve as therapeutic targets for LUAD. According to studies, stromal cells and immune cells form major components of the tissue microenvironment (TME), and immune and stromal scores are associated with clinical features as well as prognosis in LUAD [43, 44]. Using the ESTIMATE algorithm, we estimated TME scores and found that high CAG_score groups presented significantly higher immune and stromal scores than low CAG_score groups. This suggested that cuproptosis could be associated with the involvement of the TME, thus regulating LUAD occurrence and development. Besides, researchers have discovered that abnormal

immune cells promote the progression of LUAD and control the RCD like ferroptosis, and that checkpoint inhibitor-based immunotherapies have raised survival among patients with advanced cancer [21, 45, 46]. In our study, we identified that higher expression of immune cells such as NK, macrophages, Th1, and Treg as well as immune functions like APC-co-inhibition/stimulation, CCR, check-point, Type-II-IFN-response, and parainflammation were highly correlated with high CAG_score. Considering the high immune infiltration of high CAG_score was related to poor prognosis, targeting cuproptosis might be a valuable regulative strategy for immunotherapy of LUAD.

When applying the GDSC dataset to find the possible drugs, we were pleasantly surprised to find that the IC50 of 9 compounds in the low CAG_score group was significantly higher than the high CAG_score group, implying that high CAG_score patients may have greater sensitivity to these possible drugs. Furthermore, we evaluated the sensitivity to common anti-tumor drugs such as gefitinib, cisplatin, and gemcitabine in different CAG_score groups to guide clinical medication. IPS signature and the expression levels of critical ICPs such as PD-1, PD-L1, and CTLA-4 were assessed and indicated that CAG_score has the potential to determine patients who have a better response to ICIs.

Admittedly, there were several limitations suspending in our study. First, we obtained all the raw data from public databases, which may lead to bias in the analysis results. Besides, cuproptosis death is a newly discovered mechanism of programmed cell death, and there are few related studies. Last but not least, this research was conducted based on bioinformatics technology, and complementary in vivo and in vitro experimental studies are necessary to confirm our findings.

Acknowledgements

This work was supported by the Natural Science Foundation of Tianjin (19JCZDJC35500).

Disclosure of conflict of interest

None.

Address correspondence to: Peng Zhang, Department of Thoracic Surgery, Tianjin Medical University

Cuproptosis associated genes affect LUAD

General Hospital, Tianjin, China. E-mail: peng-zhang01@tmu.edu.cn

References

- [1] Blandin Knight S, Crosbie PA, Balata H, Chudziak J, Hussell T and Dive C. Progress and prospects of early detection in lung cancer. *Open Biol* 2017; 7: 170070.
- [2] Siegel RL, Miller KD, Fuchs HE and Jemal A. Cancer statistics, 2021. *CA Cancer J Clin* 2021; 71: 7-33.
- [3] Devarakonda S, Morgensztern D and Govindan R. Genomic alterations in lung adenocarcinoma. *Lancet Oncol* 2015; 16: e342-351.
- [4] Zhang C, Zhang J, Xu FP, Wang YG, Xie Z, Su J, Dong S, Nie Q, Shao Y, Zhou Q, Yang JJ, Yang XN, Zhang XC, Li Z, Wu YL and Zhong WZ. Genomic landscape and immune microenvironment features of preinvasive and early invasive lung adenocarcinoma. *J Thorac Oncol* 2019; 14: 1912-1923.
- [5] Hirsch FR, Scagliotti GV, Mulshine JL, Kwon R, Curran WJ, Wu YL and Paz-Ares L. Lung cancer: current therapies and new targeted treatments. *Lancet* 2017; 389: 299-311.
- [6] Lin JJ, Cardarella S, Lydon CA, Dahlberg SE, Jackman DM, Jänne PA and Johnson BE. Five-year survival in EGFR-mutant metastatic lung adenocarcinoma treated with EGFR-TKIs. *J Thorac Oncol* 2016; 11: 556-565.
- [7] Yang J, Qiu Q, Qian X, Yi J, Jiao Y, Yu M, Li X, Li J, Mi C, Zhang J, Lu B, Chen E, Liu P and Lu Y. Long noncoding RNA LCAT1 functions as a ceRNA to regulate RAC1 function by sponging miR-4715-5p in lung cancer. *Mol Cancer* 2019; 18: 171.
- [8] Calvayrac O, Pradines A, Pons E, Mazières J and Guibert N. Molecular biomarkers for lung adenocarcinoma. *Eur Respir J* 2017; 49: 1601734.
- [9] Fuchs Y and Steller H. Programmed cell death in animal development and disease. *Cell* 2011; 147: 742-758.
- [10] Koren E and Fuchs Y. Modes of regulated cell death in cancer. *Cancer Discov* 2021; 11: 245-265.
- [11] Ouyang L, Shi Z, Zhao S, Wang FT, Zhou TT, Liu B and Bao JK. Programmed cell death pathways in cancer: a review of apoptosis, autophagy and programmed necrosis. *Cell Prolif* 2012; 45: 487-498.
- [12] Qi X, Li Q, Che X, Wang Q and Wu G. Application of regulatory cell death in cancer: based on targeted therapy and immunotherapy. *Front Immunol* 2022; 13: 837293.
- [13] Tsvetkov P, Coy S, Petrova B, Dreishpoon M, Verma A, Abdusamad M, Rossen J, Joesch-Cohen L, Humeidi R, Spangler RD, Eaton JK, Frenkel E, Kocak M, Corsello SM, Lutsenko S, Kanarek N, Santagata S and Golub TR. Copper induces cell death by targeting lipoylated TCA cycle proteins. *Science* 2022; 375: 1254-1261.
- [14] Wang Y, Zhang L and Zhou F. Cuproptosis: a new form of programmed cell death. *Cell Mol Immunol* 2022; 19: 867-868.
- [15] Wang F, Wei XL, Wang FH, Xu N, Shen L, Dai GH, Yuan XL, Chen Y, Yang SJ, Shi JH, Hu XC, Lin XY, Zhang QY, Feng JF, Ba Y, Liu YP, Li W, Shu YQ, Jiang Y, Li Q, Wang JW, Wu H, Feng H, Yao S and Xu RH. Safety, efficacy and tumor mutational burden as a biomarker of overall survival benefit in chemo-refractory gastric cancer treated with toripalimab, a PD-1 antibody in phase Ib/II clinical trial NCT02915432. *Ann Oncol* 2019; 30: 1479-1486.
- [16] Chalabi M, Fanchi LF, Dijkstra KK, Van den Berg JG, Aalbers AG, Sikorska K, Lopez-Yurda M, Grootsholten C, Beets GL, Snaebjornsson P, Maas M, Mertz M, Veninga V, Bounova G, Broeks A, Beets-Tan RG, de Wijkerslooth TR, van Lent AU, Marsman HA, Nuijten E, Kok NF, Kuiper M, Verbeek WH, Kok M, Van Leerdam ME, Schumacher TN, Voest EE and Haanen JB. Neoadjuvant immunotherapy leads to pathological responses in MMR-proficient and MMR-deficient early-stage colon cancers. *Nat Med* 2020; 26: 566-576.
- [17] Garon EB, Rizvi NA, Hui R, Leighl N, Balmanoukian AS, Eder JP, Patnaik A, Aggarwal C, Gubens M, Horn L, Carcereny E, Ahn MJ, Felip E, Lee JS, Hellmann MD, Hamid O, Goldman JW, Soria JC, Dolled-Filhart M, Rutledge RZ, Zhang J, Luceford JK, Rangwala R, Lubiniecki GM, Roach C, Emancipator K and Gandhi L. Pembrolizumab for the treatment of non-small-cell lung cancer. *N Engl J Med* 2015; 372: 2018-2028.
- [18] Topalian SL, Hodi FS, Brahmer JR, Gettinger SN, Smith DC, McDermott DF, Powderly JD, Carvajal RD, Sosman JA, Atkins MB, Leming PD, Spigel DR, Antonia SJ, Horn L, Drake CG, Pardoll DM, Chen L, Sharfman WH, Anders RA, Taube JM, McMiller TL, Xu H, Korman AJ, Jure-Kunkel M, Agrawal S, McDonald D, Kollia GD, Gupta A, Wigginton JM and Sznol M. Safety, activity, and immune correlates of anti-PD-1 antibody in cancer. *N Engl J Med* 2012; 366: 2443-2454.
- [19] Bader JE, Voss K and Rathmell JC. Targeting metabolism to improve the tumor microenvironment for cancer immunotherapy. *Mol Cell* 2020; 78: 1019-1033.
- [20] Fridman WH, Zitvogel L, Sautès-Fridman C and Kroemer G. The immune contexture in cancer prognosis and treatment. *Nat Rev Clin Oncol* 2017; 14: 717-734.

Cuproptosis associated genes affect LUAD

- [21] Wang W, Green M, Choi JE, Gijón M, Kennedy PD, Johnson JK, Liao P, Lang X, Kryczek I, Sell A, Xia H, Zhou J, Li G, Li J, Li W, Wei S, Vatan L, Zhang H, Szeliga W, Gu W, Liu R, Lawrence TS, Lamb C, Tanno Y, Cieslik M, Stone E, Georgiou G, Chan TA, Chinnaiyan A and Zou W. CD8+ T cells regulate tumour ferroptosis during cancer immunotherapy. *Nature* 2019; 569: 270-274.
- [22] Liu Z, Zhao Q, Zuo ZX, Yuan SQ, Yu K, Zhang Q, Zhang X, Sheng H, Ju HQ, Cheng H, Wang F, Xu RH and Liu ZX. Systematic analysis of the aberrances and functional implications of ferroptosis in cancer. *iScience* 2020; 23: 101302.
- [23] Sabah A, Tiun S, Sani NS, Ayob M and Taha AY. Enhancing web search result clustering model based on multiview multirepresentation consensus cluster ensemble (mmcc) approach. *PLoS One* 2021; 16: e0245264.
- [24] Seiler M, Huang CC, Szalma S and Bhanot G. ConsensusCluster: a software tool for unsupervised cluster discovery in numerical data. *OMICS* 2010; 14: 109-113.
- [25] Li F, Wan B, He X and Li X. Identification of novel subtypes in lung adenocarcinoma: evidence from gene set variation analysis in tumor and adjacent nontumor samples. *Dis Markers* 2022; 2022: 2602812.
- [26] Du J, Tao Q, Liu Y, Huang Z, Jin H, Lin W, Huang X, Zeng J, Zhao Y, Liu L, Xu Q, Han X, Chen L, Chen XL and Wen Y. Assessment of the targeted effect of Sijunzi decoction on the colorectal cancer microenvironment via the ESTIMATE algorithm. *PLoS One* 2022; 17: e0264720.
- [27] Pang Z, Chen X, Wang Y, Wang Y, Yan T, Wan J and Du J. Comprehensive analyses of the heterogeneity and prognostic significance of tumor-infiltrating immune cells in non-small-cell lung cancer: development and validation of an individualized prognostic model. *Int Immunopharmacol* 2020; 86: 106744.
- [28] Jin Y, Wang Z, He D, Zhu Y, Chen X and Cao K. Identification of novel subtypes based on ssGSEA in immune-related prognostic signature for tongue squamous cell carcinoma. *Cancer Med* 2021; 10: 8693-8707.
- [29] Yu G, Wang LG, Han Y and He QY. clusterProfiler: an R package for comparing biological themes among gene clusters. *OMICS* 2012; 16: 284-287.
- [30] Canzler S and Hackermüller J. multiGSEA: a GSEA-based pathway enrichment analysis for multi-omics data. *BMC Bioinformatics* 2020; 21: 561.
- [31] Bi F, Chen Y and Yang Q. Significance of tumor mutation burden combined with immune infiltrates in the progression and prognosis of ovarian cancer. *Cancer Cell Int* 2020; 20: 373.
- [32] Zhuang J, Chen Z, Chen Z, Chen J, Liu M, Xu X, Liu Y, Yang S, Hu Z and He F. Construction of an immune-related lncRNA signature pair for predicting oncologic outcomes and the sensitivity of immunosuppressor in treatment of lung adenocarcinoma. *Respir Res* 2022; 23: 123.
- [33] Tang D, Chen X and Kroemer G. Cuproptosis: a copper-triggered modality of mitochondrial cell death. *Cell Res* 2022; 32: 417-418.
- [34] Xia X, Fan X, Zhao M and Zhu P. The relationship between ferroptosis and tumors: a novel landscape for therapeutic approach. *Curr Gene Ther* 2019; 19: 117-124.
- [35] Martín A, Odajima J, Hunt SL, Dubus P, Ortega S, Malumbres M and Barbacid M. Cdk2 is dispensable for cell cycle inhibition and tumor suppression mediated by p27(Kip1) and p21(Cip1). *Cancer Cell* 2005; 7: 591-598.
- [36] Oakes V, Wang W, Harrington B, Lee WJ, Beamish H, Chia KM, Pinder A, Goto H, Inagaki M, Pavay S and Gabrielli B. Cyclin A/Cdk2 regulates Cdh1 and claspin during late S/G2 phase of the cell cycle. *Cell Cycle* 2014; 13: 3302-3311.
- [37] Wu G, Wang Q, Xu Y, Li Q and Cheng L. A new survival model based on ferroptosis-related genes for prognostic prediction in clear cell renal cell carcinoma. *Aging (Albany NY)* 2020; 12: 14933-14948.
- [38] Che X, Qi X, Xu Y, Wang Q and Wu G. Using genomic and transcriptome analyses to identify the role of the oxidative stress pathway in renal clear cell carcinoma and its potential therapeutic significance. *Oxid Med Cell Longev* 2021; 2021: 5561124.
- [39] Su Z, Yang Z, Xu Y, Chen Y and Yu Q. Apoptosis, autophagy, necroptosis, and cancer metastasis. *Mol Cancer* 2015; 14: 48.
- [40] Levy JMM, Towers CG and Thorburn A. Targeting autophagy in cancer. *Nat Rev Cancer* 2017; 17: 528-542.
- [41] Oliveri V. Selective targeting of cancer cells by copper ionophores: an overview. *Front Mol Biosci* 2022; 9: 841814.
- [42] Jiang T, Fang Z, Tang S, Cheng R, Li Y, Ren S, Su C, Min W, Guo X, Zhu W, Zhang H, Hou L, Pan Y, Zhou Z, Zhang J, Zhang G, Yue Z, Chen L and Zhou C. Mutational landscape and evolutionary pattern of liver and brain metastasis in lung adenocarcinoma. *J Thorac Oncol* 2021; 16: 237-249.
- [43] Chen Z, Huang Y, Hu Z, Zhao M, Li M, Bi G, Zheng Y, Liang J, Lu T, Jiang W, Xu S, Zhan C, Xi J, Wang Q and Tan L. Landscape and dynamics of single tumor and immune cells in early and advanced-stage lung adenocarcinoma. *Clin Transl Med* 2021; 11: e350.
- [44] Chen D, Wang Y, Zhang X, Ding Q, Wang X, Xue Y, Wang W, Mao Y, Chen C and Chen Y. Characterization of tumor microenvironment in lung adenocarcinoma identifies immune sig-

Cuproptosis associated genes affect LUAD

- natures to predict clinical outcomes and therapeutic responses. *Front Oncol* 2021; 11: 581030.
- [45] Biton J, Mansuet-Lupo A, Pécuchet N, Alifano M, Ouakrim H, Arrondeau J, Boudou-Rouquette P, Goldwasser F, Leroy K, Goc J, Wislez M, Germain C, Laurent-Puig P, Dieu-Nosjean MC, Cremer I, Herbst R, Blons H and Damotte D. TP53, STK11, and EGFR mutations predict tumor immune profile and the response to anti-PD-1 in lung adenocarcinoma. *Clin Cancer Res* 2018; 24: 5710-5723.
- [46] Kang L, Miao MS, Song YG, Fang XY, Zhang J, Zhang YN and Miao JX. Total flavonoids of *Taraxacum mongolicum* inhibit non-small cell lung cancer by regulating immune function. *J Ethnopharmacol* 2021; 281: 114514.

Cuproptosis associated genes affect LUAD

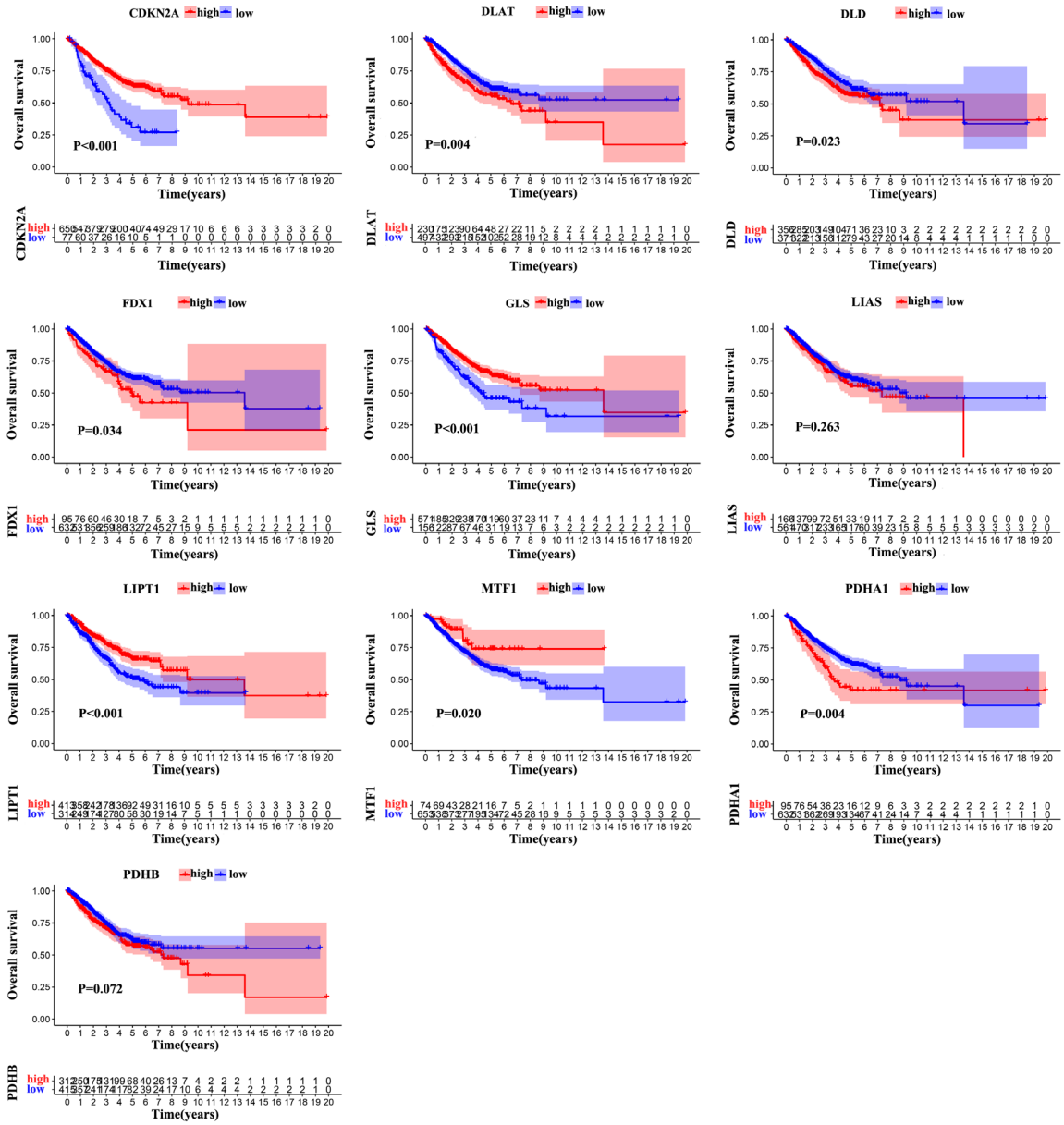


Figure S1. K-M analysis based on CAGs in LUAD cohort.

Cuproptosis associated genes affect LUAD

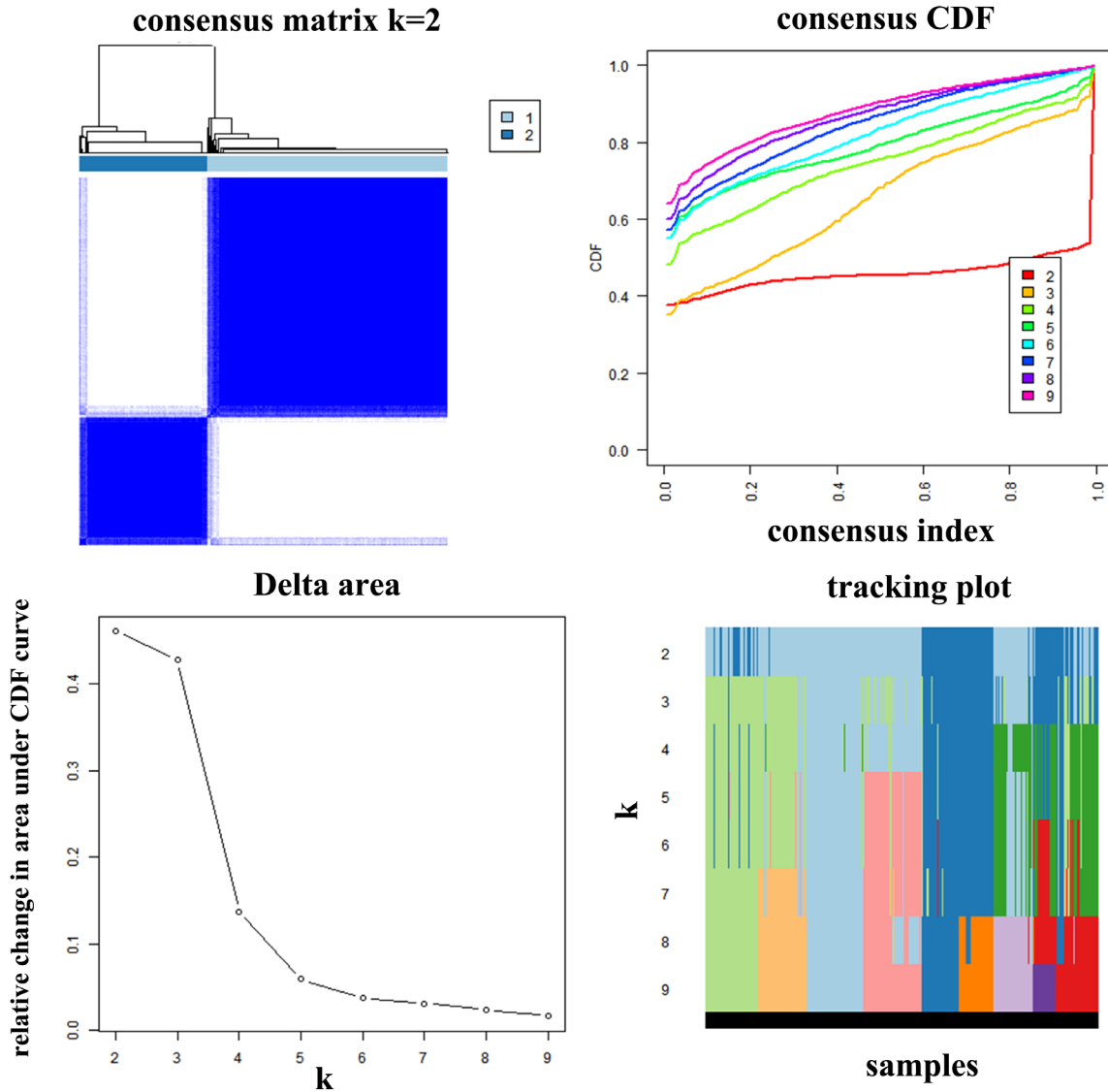


Figure S2. Identification of CAG subtypes based on expression of CAGs in LUAD cohort.

Cuproptosis associated genes affect LUAD

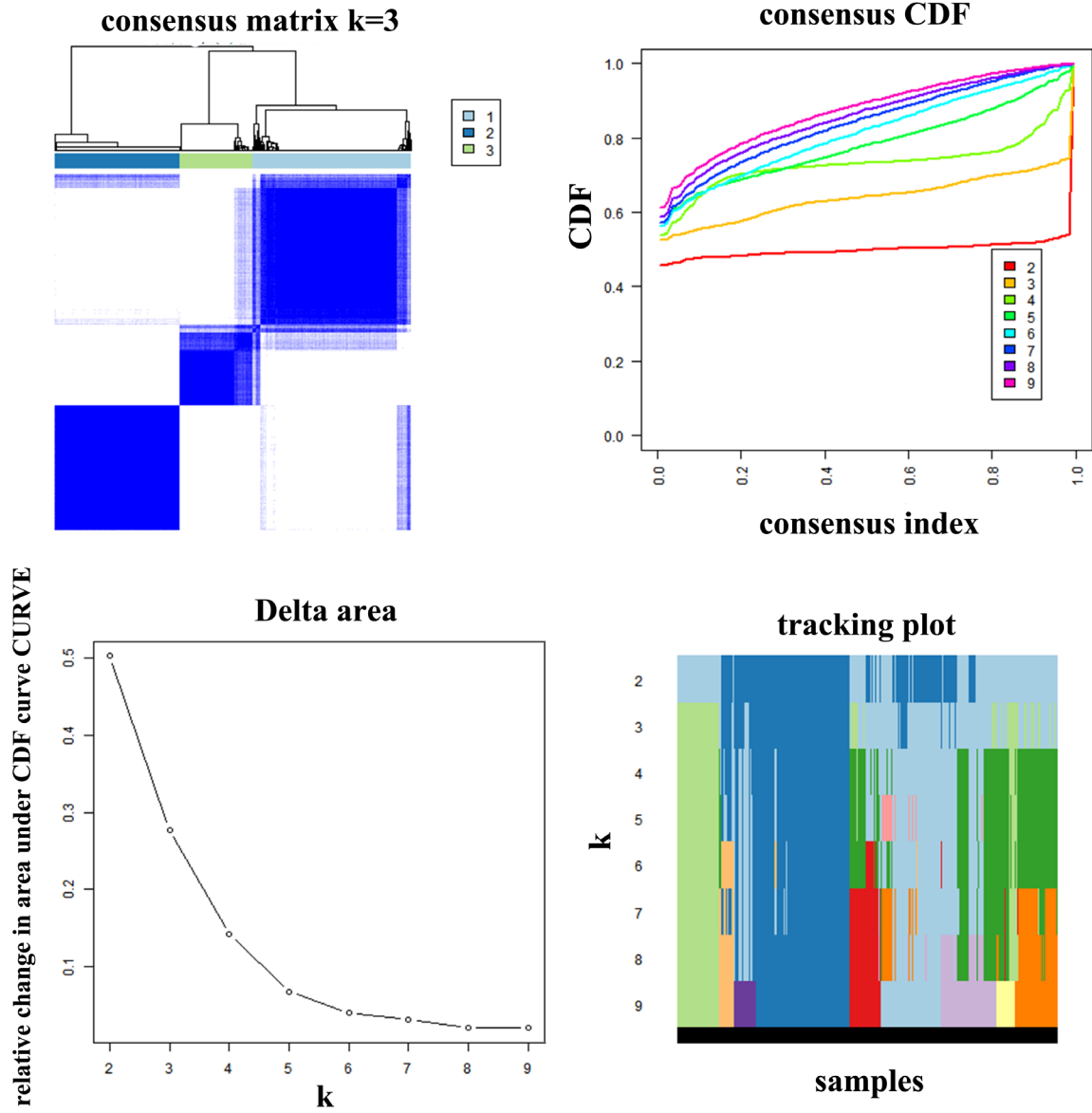


Figure S3. Identification of gene subtypes based on DEGs among two CAG subgroups in LUAD cohort.